JOURNAL OF COMPUTATIONAL PHYSICS 118, 62–72 (1995)

Numerical Methods for Nonlinear Interactions between Water Waves

H. S. ÖLMEZ* AND J. H. MILGRAM

Department of Ocean Engineering, Massachusetts Institute of Technology, Cambridge, Massachusetts 02139

Received April 27, 1993; revised September 8, 1994

Two numerical methods for studying nonlinear interactions between spatially periodic water waves of disparate length scales are explored. Both use a time-stepping procedure, but one solves the boundary value problem at each time step by a boundary integral equation and the other uses a high-order spectral method. The central issues are the restrictions on accuracy of the spectral method associated with its inherent internal perturbation expansion and the propagation of numerical boundary integral method errors from the edge of the computational domain into its interior. The spectral method was found to be accurate for larger values of the product of long-wave amplitude and short-wave number than one might expect. Two methods of correcting numerical errors at each time step in the boundary integral equation method are explored. One evaluates the vertical derivative of the velocity potential at the surface by use of computed values of the potential on the vertical sides of the domain. The other replaces computed values by interpolated values based on spatial periodicity. Using either of these allows the boundary integral method to be used for larger values of the product of long-wave amplitude and short-wave number and for steeper waves than can be handled by the spectral method, but at substantially greater computational expense.

1. INTRODUCTION

With the advance of computational capability, numerical treatment of nonlinear water wave dynamics has experienced considerable progress in recent years. For the most part, the essential nonlinear features can be considered by inviscid hydrodynamic models. These can be divided into two classes: rotational and irrotational. Here we consider the latter which is appropriate for focusing on interactions between waves. The solution quantities usually sought are the free-surface elevation and the velocity potential distributions.

Computational methods for wave–wave interactions can be carried out in water of finite depth with a lower boundary for the computational domain or for infinite depth where the domain depth is made large enough for the fluid motion beneath it to be negligible. Since the domain size must be finite out of necessity, consideration at the vertical boundaries at its horizontal extents is required.

For some transient wave problems, initial conditions with no flow or wave elevation at the domain edges can be used with the computation terminated before there is significant wave motion at the edges. However, in most computational wave–wave interaction problems the edges are involved. One example is wave motion in a region bounded by walls which leads to Neumann boundary conditions on these walls. Problems with progressive waves generally involve periodicity conditions on the boundaries and it is these problems that are of particular interest to us here.

Although there are some exceptions, most numerical methods for wave–wave interactions in finite domains have maximum numerical error at or near the domain edges. These errors may be of small consequence when a boundary problem has to be solved only once. However, solutions to nonlinear wave–wave interaction problems are usually obtained in the time domain by time-stepping the governing equations with the boundary value problem solved at each time step. This can lead not only to an increasing error with each time step, but also to propagation of the error to more interior parts of the computational domain. As a result, it is important to develop and use numerical solution methods with the smallest possible numerical error over the entire domain.

Most of the developmental efforts for numerical solutions to wave–wave interaction problems have been for two-dimensional flow. This limits consideration to waves which all propagate in the same direction. Our interest is in three-dimensional problems. They have greatly increased demands on computational resources. The combination of the needs for very small numerical error in solution of the wave interaction boundary value problems and for carrying out the solutions in three dimensions has led to the study and development of the numerical methods that are described here.

Two numerical methods for wave–wave interaction problems with periodic boundary conditions have had considerable development. One, called the spectral method, is a high-order perturbation theory expansion for the solution which is specified as the sum of the contributions at each order [2, 20]. The

* Present address: Bilkent University, Faculty of Business Administration, Bilkent 06533, Ankara, Turkey.

0021-9991/95 $6.00

solution at each order is represented as a sum of modes, each of which varies sinusoidally in the horizontal directions and exponentially in the vertical direction. Values of the velocity potential and its vertical derivative at the position of the undisturbed free-surface are expanded in Taylor series to obtain the needed estimates of these functions on the displaced free-surface.

When the waves are steep, or when interactions between waves of disparate length scales are considered, the validity of the spectral method has been questioned [9]. For example, in the interaction between a long wave of amplitude a_l and wavenumber k_l and a short wave having amplitude a_s and wavenumber k_s, we would like to examine cases for which $a_l k_s > 1$. In other words, the long-wave amplitude is not necessarily small in comparison to the short wave length. There is no guarantee that continuations of short-wave quantities over distances of long-wave amplitudes by truncated Taylor series are accurate under these circumstances.

The other numerical method is the boundary integral equation method (BIEM) in which Green's theorem is used after each time step to compute normal velocities on the free-surface. This approach avoids the limitations of perturbation theory, but can have excessive errors at the domain edges. One way of implementing the BIEM is to use a Green function that is spatially periodic for two-dimensional problems and spatially doubly-periodic for three-dimensional problems. In these implementations, detailed integrations of the Green function over surface panels in the domain are carried out and the sum of the infinite series associated with point sources and dipoles at all surface image points is used to effectively remove the edges of the computational domain. We shall see that this approach introduces excessive errors near the domain edges due to the inherent approximation of singularity panels by point singularities outside the computational domain.

In this paper, we develop methods of correcting BIEM results at domain edges so the process can be used effectively in time-stepped solutions to nonlinear wave–wave interaction problems in both two and three dimensions. The process is applied to three problems, one of which has a well-known solution which can be used as a basis for comparison.

The same problems are solved here by a higher-order spectral method. Although this cannot be used for waves that are quite as steep as can the BIEM, the steepnesses and values of $a_l k_s$ for which the spectral method is accurate are remarkably large.

The two principal contributions here for computations of nonlinear wave interactions are the edge correction methods for the BIEM and the demonstration of the accuracy of the spectral method for interactions between waves of disparate length scales.

2. DESCRIPTION OF THE NUMERICAL METHODS

Time-stepping of the free-surface position, ζ and of the value of the velocity potential, ϕ on the free-surface is done with the free-surface boundary conditions:

$$\frac{\partial \zeta}{\partial t} = \frac{\partial \phi}{\partial z} - \tilde{\nabla}\phi \cdot \tilde{\nabla}\zeta \quad \text{at } z = \zeta, \tag{1}$$

$$\frac{\partial \phi}{\partial t} = -g\zeta - \frac{1}{2}\tilde{\nabla}\phi \cdot \tilde{\nabla}\phi + \frac{1}{2}\left(\frac{\partial \phi}{\partial z}\right)^2 \quad \text{at } z = \zeta, \tag{2}$$

where $\tilde{\nabla} = (\partial/\partial x, \partial/\partial y)$ denotes the horizontal gradient. In order to continue the time-evolution process, updated values of ϕ_z at the free-surface must be determined after each time step. The difference between the spectral and the boundary integral equation methods lies in the way ϕ_z is determined.

The time integration of the free-surface boundary conditions is done numerically using a high-order scheme. For our calculations with the spectral method, we adopted the fourth-order, explicit Runge–Kutta method [6] with a constant time step. For the BIEM applications, a fourth-order, multi-step Adams–Bashforth–Moulton method [6] is preferred over Runge–Kutta due to its computational efficiency as the numerical technique is computationally expensive. Various time step sizes were tested in each of our calculations. A general finding was that a good time step size is 2–3% of the shortest fundamental wave period in the problem under consideration. No significant gains in accuracy were achieved with shorter time steps.

During the time-stepping procedure, a high-wavenumber instability on the free-surface develops which, if not suppressed, eventually causes the numerical scheme to break down. This type of instability, often referred to as sawtooth, has been reported by several investigators [3, 4, 10, 12, 19]. We adopted a fast Fourier transform (FFT) technique by which all the high wavenumber instabilities are filtered out. The surface wave elevation and the velocity potential are transformed into the Fourier space by a two-dimensional FFT, and then all the higher-order harmonics that are above the wavenumber at which the instability is detected are filtered out. Then transforming back into the physical space by an inverse FFT, the computations can be carried out for the succeeding time steps. A mathematically equivalent procedure is direct spatial filtering. However, the required two-dimensional convolutions are more demanding of computer time than are the Fourier transforms and wavenumber domain cutoffs that we have used. The global accuracy of the numerical scheme is monitored by computing the total energy and the horizontal momenta. These quantities are typically maintained to within 1%.

2.1. *Spectral Method*

Dommermuth and Yue [2] and West *et al.* [20] have developed a high-order spectral method for the study of nonlinear gravity waves. These references provide complete descriptions so we only summarize the method here.

The spectral method differs from the direct numerical method in the way that it evaluates the vertical derivative of the potential

after each time step. The velocity potential is expressed in terms of a perturbation series of the free wave modes expanded to an arbitrary order in wave steepness about the reference surface, $z = 0$. The objective is to express the vertical velocity in terms of the surface potential and the wave elevation. Once this is done, time-forwarding of the evolution equations can proceed. The spectral method presupposes that the velocity potential can be expanded as a regular perturbation expansion in the form

$$\Phi(\mathbf{x}, z, t) = \sum_{m=1}^{M} \Phi_m(\mathbf{x}, z, t), \tag{3}$$

where $\mathbf{x} = (x, y)$ and M denotes the order of expansion adopted in the procedure. Following Dommermuth and Yue, each Φ_m is expanded in a Taylor series about $z = 0$ and the surface potential is obtained as

$$\Phi_S(\mathbf{x}, t) = \Phi(\mathbf{x}, \zeta, t) = \sum_{m=1}^{M} \sum_{k=0}^{M-m} \frac{\zeta^k}{k!} \frac{\partial^k}{\partial z^k} \Phi_m(\mathbf{x}, 0, t). \tag{4}$$

Expanding Eq. (4) and collecting terms at each order, we get the following sequence of equations for the unknown Φ_m's in terms of the surface potential $\Phi_S(\mathbf{x}, t)$:

$$\Phi_1(\mathbf{x}, 0, t) = \Phi_S(\mathbf{x}, t), \tag{5}$$

$$\Phi_m(\mathbf{x}, 0, t) = -\sum_{k=1}^{m-1} \frac{\zeta^k}{k!} \frac{\partial^k}{\partial z^k} \Phi_{m-k}(\mathbf{x}, 0, t), \quad m = 2, ..., M. \tag{6}$$

The velocity potential at each order m (assuming periodic boundary conditions) for a wave field composed of N free wave modes can be expressed by the sum

$$\Phi_m(\mathbf{x}, z, t) = \sum_{n=1}^{N} \phi_{m,n}(t) e^{|\mathbf{k}_n| z} e^{i\mathbf{k}_n \cdot \mathbf{x}}, \quad m = 1, 2, ..., M \tag{7}$$

where the $\mathbf{k}_n$'s are the wavenumber harmonics of the horizontal domain, $\mathbf{k} = (k_x, k_y)$, and deep water is implied. The modal amplitudes, $\phi_{m,n}$, are found by substituting Eq. (7) into (5) and (6), and solving for the unknowns. The vertical velocity is then approximated by

$$\left(\frac{\partial \phi}{\partial z}\right) = \sum_{m=1}^{M} \sum_{k=0}^{M-m} \frac{\zeta^k}{k!} \left[\frac{\partial^{k+1}}{\partial z^{k+1}} \sum_{n=1}^{N} \phi_{m,n}(t) e^{|\mathbf{k}_n| z} e^{i\mathbf{k}_n \cdot \mathbf{x}} \right]_{z=0}. \tag{8}$$

Fast Fourier transforms are employed for moving back and forth between the physical and Fourier domains. For the time-stepping procedure, all the horizontal gradients of the surface potential and the wave height are performed in the Fourier domain. Starting with prescribed initial conditions for $\Phi_S(\mathbf{x}, t_0)$ and $\zeta(\mathbf{x}, t_0)$, the free-surface boundary conditions are integrated in time over equally spaced collocation points, and the new values of the surface potential and the free-surface shape are computed in the physical domain. Based on the above approach, we prepared a computer algorithm for solutions of nonlinear wave problems presented herein.

2.2. *Boundary Integral Equation Method*

One way to compute the velocity potential or its normal gradient for potential-flow problems is the direct application of Green's theorem. We consider solutions for the velocity potential, ϕ, and its derivatives that are square-integrable in a simply-connected domain whose surface is denoted by S. Upon the application of Green's second identity, the value of ϕ at any point on the boundary is given by the integral equation [22]

$$-2\pi\phi(\mathbf{p}) = \iint \phi(\mathbf{q}) \frac{\partial G(\mathbf{p}, \mathbf{q})}{\partial n(\mathbf{q})} dS(\mathbf{q}) - \iint G(\mathbf{p}, \mathbf{q}) \frac{\partial \phi(\mathbf{q})}{\partial n(\mathbf{q})} dS(\mathbf{q}), \tag{9}$$

where the first integral is in the sense of a Cauchy principal value and excludes itegration over the source point $\mathbf{q} = (\xi, \eta, \zeta)$, where the singularity is located. $\mathbf{p} = (x, y, z)$ is the field point. $G(\mathbf{p}, \mathbf{q})$ is the three-dimensional free-space Green function defined by

$$G(x, y, z, \xi, \eta, \zeta) = \frac{1}{|\mathbf{p} - \mathbf{q}|} = [(x - \xi)^2 + (y - \eta)^2 + (z - \zeta)^2]^{-1/2}, \tag{10}$$

where $|\mathbf{p} - \mathbf{q}|$ is the distance between the source and field points.

We will solve the integral equation (9) numerically by discretizing the boundary S into N quadrilateral panels and by satisfying the equation at a prescribed collocation point on each panel. The simplest form is to consider the singularity strengths to be constant on each panel and each panel to lie in a plane. Although the approach may seem crude, the comparisons we shall provide show that the results are remarkably accurate. Each integral in Eq. (9) now depends only on the form of the Rankine source Green function in Eq. (10) and the geometry of panels. Explicit expressions for these integrals, which we have used in our numerical implementation, are given by Newman [14].

Some aspects of our BIEM are new and different from previous developments so we will describe our approach in some detail. We consider the free-surface flow in a bounded region composed of a free-surface and four vertical faces. Since deep water waves are considered, the computational domain can be freed of the bottom face, provided that the domain is deep enough so that there is no flow at its bottom. Spatially periodic solutions are considered so that the boundary conditions on the side faces become periodicity conditions. The vertical faces are partitioned into panels by a rectangular grid and the periodicity conditions are invoked at the center of each panel. The free-

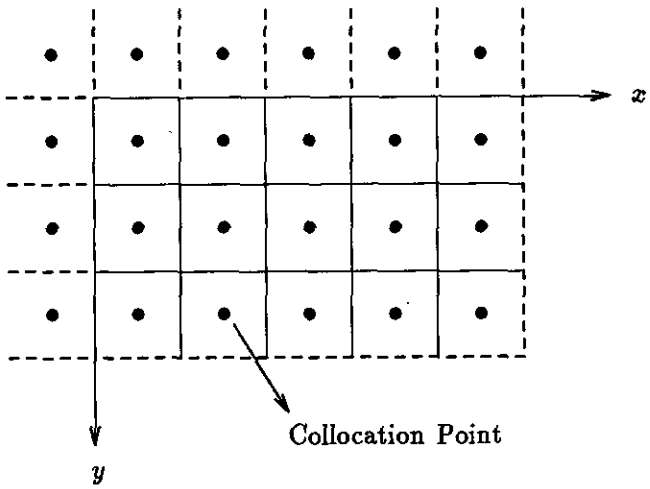

FIG. 1. Collocation points on the free-surface (the computational domain is to the lower right of the axes).

surface is partitioned into subsurfaces by a rectangular grid with constant spacing in each of the x- and y-directions. The free-surface shape changes with time, and at each time step, each subsurface is approximated by a best-fit tilted quadrilateral panel by the method of Hess and Smith [8]. Collocation points are chosen at the centroid of each panel where the boundary conditions will be invoked to update the vertical surface motion and the velocity potential on the free-surface. For the next time step, ϕ_z is determined by solving the integral equation (9) and the process is repeated, but one intermediate step must first be carried out. Time-stepping by use of the free-surface boundary conditions provides elevations at the collocation points. However, to generate the set of tilted quadrilateral panels on the free-surface needed for solving the integral equation (9), elevations at the panel *corners* are required. The numerical grid generation for the corner heights is done through a bicubic interpolation of the wave elevations prescribed at the collocation points. The interpolation function matches the surface elevation at each collocation point, and the elevation and its gradients change in a continuous manner from one grid point to the other. The numerical implementation in Chapter 3 of Press *et al.* [17] is adopted for the above procedure. In order that this process give accurate results at those corner points along the domain edges as well as at interior corner points, we apply the bicubic interpolation over a surface region larger than the domain by extending it on the basis of spatial periodicity (Fig. 1).

A well-known problem in numerical applications of the BIEM, although not studied in detail by others, is the rather poor accuracy along the edges of the boundaries. The discontinuity in the normal direction and in the normal gradient of the potential at the edge elements impairs the accuracy of numerical solutions to boundary integral equations [7, 18]. The importance of the accuracy along the edge panels on the free-surface lies in the fact that errors there propagate through the computational domain during the time-stepping process because of the hyperbolic nature of the boundary conditions. Use of doubly-periodic Green functions for three-dimensional problems eliminates the need for the vertical sides of the computational domain [21]. This approach, however, can lead to large errors at the edges as is shown in the Appendix.

For testing techniques to diminish the local errors at the edge elements, we applied the BIEM to a uni-directional Stokes wave with a steepness of 0.1. Using 25 panels along the wave propagation direction and 20 uniformly spaced elements along the depth, taken as half the wavelength, we computed the error in the normal velocity on the free-surface relative to the exact, theoretical values. The maximum relative error occurs at the corners of the domain with a value of 4.5%. Increasing the number of elements along the depth improves the accuracy along the edges. This approach, however, becomes impractical, perhaps prohibitive, for cases that require larger domains with more elements on the boundaries due to rapid increase in the computational expense. On the other hand, we can achieve further reductions in the edge errors with the same number of elements by use of a nonuniform spacing in the vertical discretization. Considering the exponential decay in the velocity potential away from the free-surface, it is anticipated that a panel distribution that provides more elements near the surface will improve the accuracy of the solution near the domain edges. We tried a quarter-period cosine-spacing distribution along the depth. This scheme generates a grid of the form in the vertical direction

$$z_n = h \cos\left(\frac{n\pi}{2N_z}\right) - h \quad \text{for } n = 0, ..., N_z, \tag{11}$$

where h is the depth and N_z is the number of elements in the z-direction. This nonuniform vertical spacing with N_z held fixed at 20 reduced the error at the corners to 1.1%. Considering the exponential decay with depth for deep water waves, a welcome feature of the cosine-spacing distribution is that it provides a better representation of the potential and its normal gradient in regions of rapid variations. For applications which involve several wave components, the depth of the domain is determined by the maximum wavelength in the field. In the presence of disparate length scales, a cosine-spacing distribution increases the density of the collocation points near the free-surface, and thus provides better spatial resolution for the smallest wavelength involved. In general, we used the cosine-spacing on vertical faces. One exception is that we used uniform spacing to investigate the influence of domain depth, since this provides more panels near the bottom.

We studied two techniques to further diminish the local error on the edge panels without materially increasing the computational effort. The first technique is based on our finding that the accuracy in the computed velocity potential on the vertical

faces, unlike its normal gradient, is fairly accurate throughout the entire depth. Hence, the vertical derivative can be accurately calculated numerically between collocation points on the vertical faces. In the first technique we extrapolate the vertical derivatives up to the surface with a second-order numerical extrapolator. Having computed the vertical gradient of the velocity potential on the free-surface for all the inner points, we can now accurately compute the vertical gradient of the potential on the edge panel, which is where the error in the solution was maximum, by a cubic interpolation using all the inner points and the ones computed by extrapolation from the sides.

The second technique we implemented does not use the potential on the vertical sides, but uses all the collocation points on the free-surface, except the ones at the edges, to form a cubic spline for the normal velocity on the surface. An essential feature of this process is fitting each spline over a length that exceeds the domain length by using the periodicity condition to obtain values outside the domain. Then we evaluate the normal velocity at the edge points by the interpolation provided by the cubic spline function.

Both of the edge correction techniques performed well in reducing the local error at the edges and provided much improved overall accuracy for the solution. The application of the second technique to our Stokes wave problem reduced the maximum error at the corners from 1.1% to 0.5%. Time-domain simulations of exact, progressive Stokes waves show this level of error to be acceptable in the sense that the error does not grow materially when the computation is extended over several wave periods.

Both edge correction techniques have been used in our applications. Having similar characteristics, one is not really superior to the other. The selection of the method depends more on the specific application. For example, the second technique is difficult to implement when only a few elements are needed in the transverse direction along which a cubic interpolation is not suitable due to sparsity of the control points. This applies to time-domain simulation of two-dimensional waves with our three-dimensional codes.

3. NUMERICAL RESULTS

The fineness of the spatial discretization is necessarily a compromise between accuracy and computational expense. The effect of the spatial discretization in horizontal directions on the surface will be investigated in our subsequent application of the BIEM to Stokes waves. This will form the basis of our spatial discretization in the other numerical applications of the method. The spacing along the x- and y-directions on the vertical sides of the domain are determined by the spacing used on the free-surface along the same directions. The depth of the domain must be selected such that no significant improvements in accuracy result from making it deeper. This depth is expected to be on the order of one-half a wavelength, where the velocity potential is about 4% of its value at the surface. To determine the sensitivity of numerical calculations to domain depth, we applied the BIEM to a uni-directional Stokes wave with a steepness of 0.1 and used 25 uniformly spaced elements in each horizontal direction. We used uniformly spaced elements in the vertical direction along which the local grid size was selected to be $\frac{1}{40}$ of the wavelength. Using different domain depths, we computed the normal velocity $\tilde{\phi}_n$ on the free-surface and compared it with the exact, theoretical one, ϕ_n. The RMS relative error for the normal velocity on the free-surface was evaluated as

$$\text{RMS-Error} = \left(\frac{1}{N_s} \sum_{i=1}^{N_s} \left[\frac{(\tilde{\phi}_n)_i - (\phi_n)_i}{(\phi_n)_{\max}} \right]^2 \right)^{1/2}, \qquad (12)$$

where $(\phi_n)_{\max}$ is the maximum normal velocity and N_s is the total number of nodes on the free-surface. The RMS error drops to a nearly constant value of 0.34% at a water depth of 40% of the wavelength. In all of our subsequent applications, however, to be conservative on the side of accuracy the domain depth will be set to 50% of the longest wavelength involved in the wave field.

We first applied our three-dimensional programs to two-dimensional problems for the simplest comparisons. To assess the accuracy of both methods, time domain simulations of exact, progressive Stokes waves were conducted for a variety of wave steepnesses. A second two-dimensional example was the interaction of long and short waves that propagate in the same direction. We then applied the methods to a three-dimensional problem in which a short wave rides on the surface of a long wave with perpendicular propagation directions.

3.1. *Stokes Waves*

To test the accuracy of the numerical implementations, we conducted a series of runs for time-domain simulations of steadily progressing Stokes waves of finite amplitude. For the comparison we used exact Stokes waves evaluated by the method of Monkmeyer and Kutzbach [13]. This gave results for nonlinear period and phase speed convergent to 10 significant figures up to $\varepsilon = 0.4$ which corresponds to 90% of the limiting Stokes steepness.

A Stokes wave with a wavelength of 2π is chosen for the numerical computations. The spatial resolution along the wave propagation direction is determined by 16, 32, and 64 panels. Only 5 panels are used in the transverse direction as this is a uni-directional wave. A depth of half the wavelength is discretized into 20 elements with a quarter-period cosine-spacing distribution. Table I is a list of the runs we conducted with the BIEM. In this table, N_x denotes the number of panels per wavelength and T refers to the nonlinear wave period. We provide the average and maximum relative errors (on a percentage basis) for each run computed as

TABLE I

List of Runs Done for the Stokes Wave Simulations Using the BIEM

Run	Steepness	N_x	Period ($\sqrt{gk}T$)	Time step	Avg. error	Max. error
1	0.10	16	6.2518563271	T/20	1.92%	3.47%
2	0.10	16	6.2518563271	T/40	1.90%	3.46%
3	0.10	32	6.2518563271	T/40	0.59%	0.83%
4	0.20	32	6.1587600708	T/40	0.66%	0.86%
5	0.20	64	6.1587600708	T/80	0.10%	0.15%
6	0.30	64	6.0067763329	T/80	0.15%	0.35%
7	0.40	64	5.8085861206	T/80	0.36%	1.34%

$$\text{Relative Error} = 100\frac{|\zeta - \tilde{\zeta}|_{\max}}{|\zeta|_{\max}}, \tag{13}$$

where ζ is the exact, and $\tilde{\zeta}$ is the computed wave profile.

Time-domain simulations of the Stokes waves were conducted for one wave period. Table I reveals that the spatial resolution is the key parameter for accurate computations of the surface profile. For a wide range of steepnesses, 64 control points per wavelength provided reasonable numerical accuracy. For $\varepsilon = 0.4$, the maximum steepness for which we obtained convergent results for the "exact" method of Monkmeyer and Kutzbach [13], we calculated the maximum relative error to be 1.34%. In view of the spatial resolution adopted in the computations, the accuracy of the BIEM for 90% of the limiting Stokes steepness is considered satisfactory.

To demonstrate the accuracy of the spectral method, we carried out the simulation of a Stokes wave with steepnesses 0.3, 0.35, and 0.4 for one wave period. The computational parameters are shown in Table II. N_x is the number of equally spaced Eulerian points on the free-surface, and M is the order. The spectral method performed well for steepnesses up to 0.35. For steepness 0.4, as the simulation progressed, a sawtooth instability in the lower wavenumber components appeared and soon thereafter computations broke down. This is consistent with the findings of Dommermuth and Yue [2] that for steepnesses beyond 0.35, convergence is poor and eventually fails.

TABLE II

List of Runs Done for the Stokes Wave Simulations Using the Spectral Method

Run	Steepness	N_x	M	Time step	Avg. error	Max. error
1	0.30	32	10	T/40	0.054%	0.108%
2	0.30	32	10	T/80	0.045%	0.095%
3	0.30	64	10	T/80	0.009%	0.026%
4	0.35	64	10	T/80	0.080%	0.360%
5	0.40	128	10	T/80	—	—

Thus, the spectral method can be used for rather steep waves, but not quite as steep as those that our BIEM can handle.

3.2. *Two-Dimensional Long–Short Wave Interactions*

It is well known that short waves riding on much longer waves tend to become shorter and steeper at the crests of the long waves, and longer and less steep at the troughs. This was first predicted by Longuet-Higgins and Stewart [11] using a perturbation approximation correct to second order. For numerical calculations in this section, we shall consider the modulation of a short wave on the surface of a longer wave and determine the spatial changes in the wavenumber of the short-wave component when both waves propagate in the same direction. We adopt a long/short wavelength ratio of $\lambda_l/\lambda_s = 8$ and a short-wave steepness of $a_s k_s = 0.05$. A wide range of steepnesses from 0.05 to 0.35 is examined for the long-wave component. Thus, values of $a_l k_s$ up to 2.8 are considered. This is surely too large for second-order perturbation theory to be accurate, but it should be well handled by the BIEM and it provides a good opportunity to assess the accuracy of the high-order spectral method.

For the BIEM, the free-surface geometry is approximated by 64 elements in the wave propagation direction for long-wave steepnesses 0.05 through 0.15. We use 128 elements for steepnesses greater than 0.15. Along the depth, which is half the wavelength of the long wave, 20 elements are used with a quarter-period cosine-spacing distribution. As both waves travel in the same direction, only 5 elements are used in the transverse direction. For the spectral method, the same number of elements are used on the free-surface for the corresponding long-wave steepnesses. For both methods, smoothing is applied at every time step such that wavenumbers above the 16th harmonic of the fundamental are filtered out. A time step of $\frac{1}{80}$ of the nonlinear long-wave period is found to be quite satisfactory and used for both methods.

The initial conditions used are the superposition of a sinusoidal short wave on a long, fully nonlinear Stokes wave. The time evolution was carried out for 1.6 short wave periods. Figure 2 shows the time evolution of the short wave amplitude, which was determined by a spatial Fourier analysis after each time step, for a long-wave steepness of 0.2. The BIEM and spectral method are in excellent agreement.

Figure 2 shows that the short-wave amplitude diminishes from its initial value when the waves interact. This is due to a third-order interaction between the waves as explained by Ölmez [16]. The responsible third-order wave here is proportional to the short-wave amplitude and to the square of the long-wave amplitude. The effect is well known when a single wave component interacts with itself at the third-order [5] and is then called the "Stokes effect."

For several values of long-wave steepnesses, Fig. 3 gives the spatial changes in the wavenumber of the short wave at crest and at the trough of the long wave. They were determined

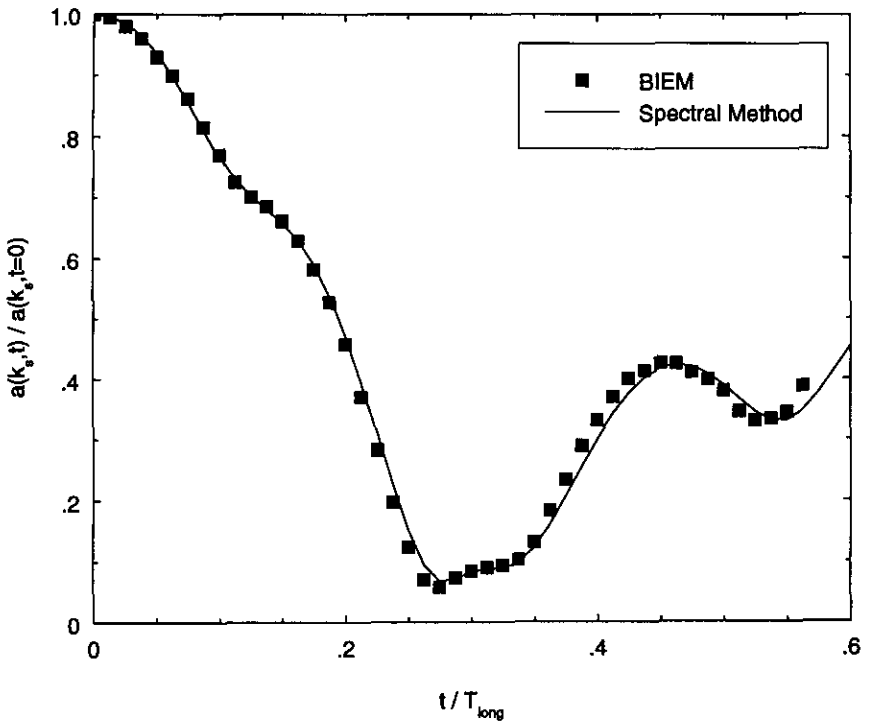

FIG. 2. Time history of the Fourier amplitude of wavenumber k_s on the surface of a long-wave with steepness 0.2.

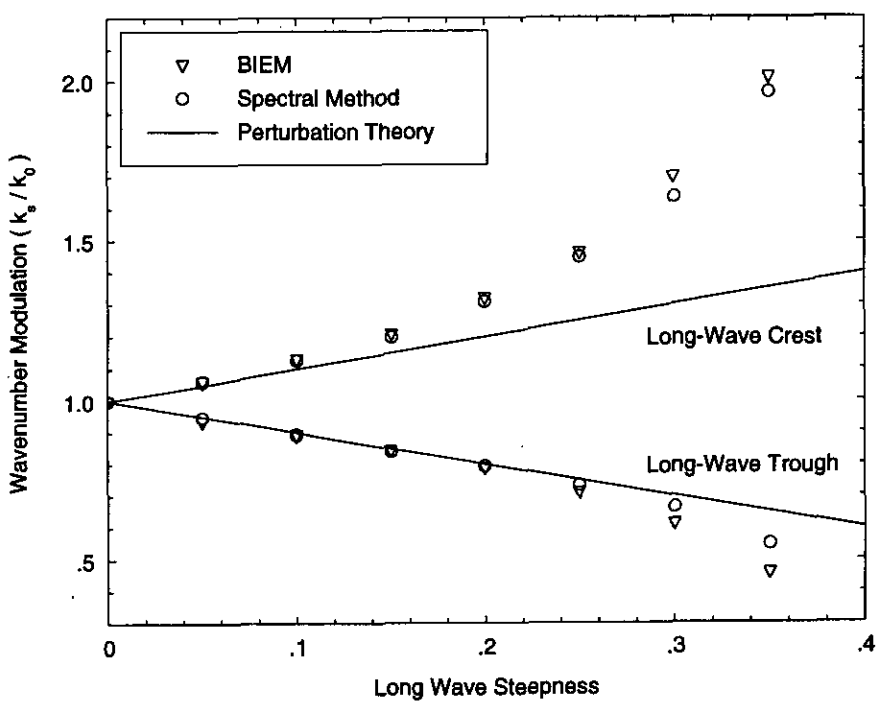

FIG. 3. The increase/decrease of the short wavenumber at the crest/trough of the long wave.

TABLE III

Contribution to the Vertical Velocity at Each Order in the Expansion

Order (M)	1	2	3	4	5	6
Ratio (%)	4.8	12.7	32.5	31.6	15.5	2.9

from the wave profile by filtering out the long-wave component and measuring the zero-crossing distances of the remaining short wave. When the long-wave steepness is small (for steepnesses smaller than 0.1), the second-order perturbation theory is in good agreement with the numerical calculations as expected. The agreement between the spectral method and the BIEM is remarkably good up to a long-wave steepness of 0.25 for which $a_l k_s = 2.0$. For larger long-wave steepnesses, the differences in the numerical methods become noticeable, such that for a long-wave steepness of 0.35, the numerical results differ by as much as 17%. This is consistent with our findings from computations with Stokes waves and attributed to the steepness exceeding the region of validity of the spectral method. It is really quite remarkable that the spectral method is accurate for $a_l k_s$ as large as 2.0, in view of the fact that it involves estimation of short-wave surface properties from a Taylor series based on derivatives that are 40% of the short-wave lengths distant from the surface. It is enlightening to investigate why this is so. To do this, we have done a Fourier analysis of the contribution to the vertical velocity at each order and have picked out the Fourier amplitudes associated with the short wave. Table III shows the contribution at each order to the total vertical velocity with $M = 6$ for a long-wave steepness of 0.25. Although the largest contributions to the velocity come from the third- and fourth-order terms, convergence is achieved rapidly as higher order terms are included. Even though the sixth-order is only two orders removed from the very influential fourth-order term, it contributes to only 2.9% of the solution. For this long-wave steepness, the spectral method compares favorably with the BIEM because the terms that are of large magnitude are captured in the perturbation expansion. Brueckner and West [1] indicate that the spectral method could be better for long–short wave interactions than might first be thought because of the cancellation of terms that become large at large expansion distances. Although our results do not prove the contention of Brueckner and West, they certainly help support them. On the other hand, it is important to note that convergence of the spectral method does not guarantee that it converges to the exact solution in all respects. As an example, for the long–short wave interaction considered here, with a long-wave steepness of 0.30, we found that the contribution to the velocity at the eighth-order is 1% of the total. Despite satisfactory convergence, results of the spectral method for the modulated wavenumber deviate from those of the BIEM at this steepness by about 6% as is evident from Fig. 3. This demonstrates that there is a limit to wave steepness for which the spectral method is valid, but it can be accurate for larger steepnesses than might have been expected heretofore for wave problems of disparate length and amplitude scales.

3.3. *Three-Dimensional Long–Short Wave Interactions*

Although we used a three-dimensional BIEM for the preceding calculations, the nature of the problems was essentially two-dimensional. For a comparison between the numerical methods for an intrinsically three-dimensional situation, we computed the free-surface profiles when the short wave propagates at an angle of $\alpha = 90°$ with respect to the propagation of the long wave. The calculations were carried out for one long-wave period. The short- and long-wave steepnesses were 0.05 and 0.2, respectively. Again, we set $\lambda_l/\lambda_s = 8$. For the spectral method with $\alpha = 90$, we set $M = 6$, and used 32 and 16 points in the x- and y-directions with corresponding filtering at the 10th- and 5th-orders. For the BIEM, the same number of elements on the surface is used with the same smoothing parameters. An example is shown in Fig. 4 which gives the short-wave profile along its propagation direction over the zero-crossing position of the long wave, after the waves have evolved for one long-wave period. Results from the BIEM and from the spectral method are very nearly identical. They differ by only about 0.3% of the long-wave amplitude. Although the BIEM can represent wave systems almost up to their limiting steepnesses, the faster computing spectral method does very well for this moderate steepness of 0.2.

Figure 5 shows the spectral method result for the short-wave profile at locations of the crest and the trough of the long wave, again after the wave system has evolved for one long-wave period. In this figure, the mean value, which is mainly the long-wave elevation, has been subtracted from each profile so the modulation of the short wave by the long wave can be easily seen. This figure shows the applicability of the numerical methods for computing amplitude modulations.

4. CONCLUSIONS

The main objectives of the present work were to develop the three-dimensional direct method and to compare its performance with that of a spectral method which utilizes the presumptions of perturbation theory, but which includes perturbations of very high order. To the best of our knowledge, this is the first effort towards comparing the computations of nonlinear wave interactions from the spectral method against a direct numerical technique (BIEM) that is not subject to the restrictions of perturbation theory.

Two important contributions of the present study can be summarized as follows:

- We developed a new technique for very effectively minimizing errors at the edges of a computational domain for three-dimensional boundary integral equation methods.

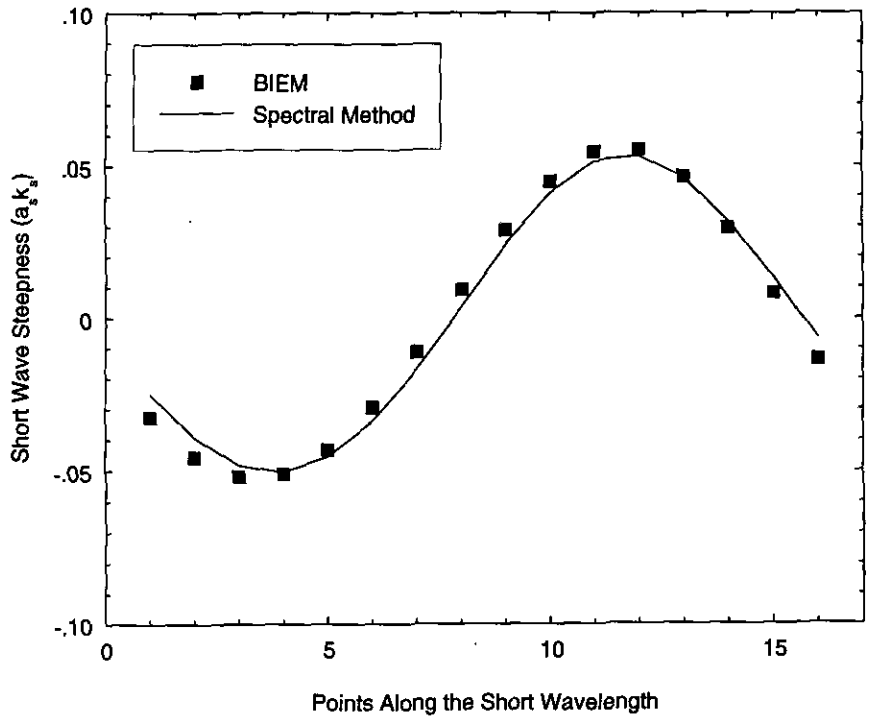

FIG. 4. Elevation vs distance in short wave propagation direction over zero-crossing location of a long wave of steepness 0.2 after an evolution of one long wave period.

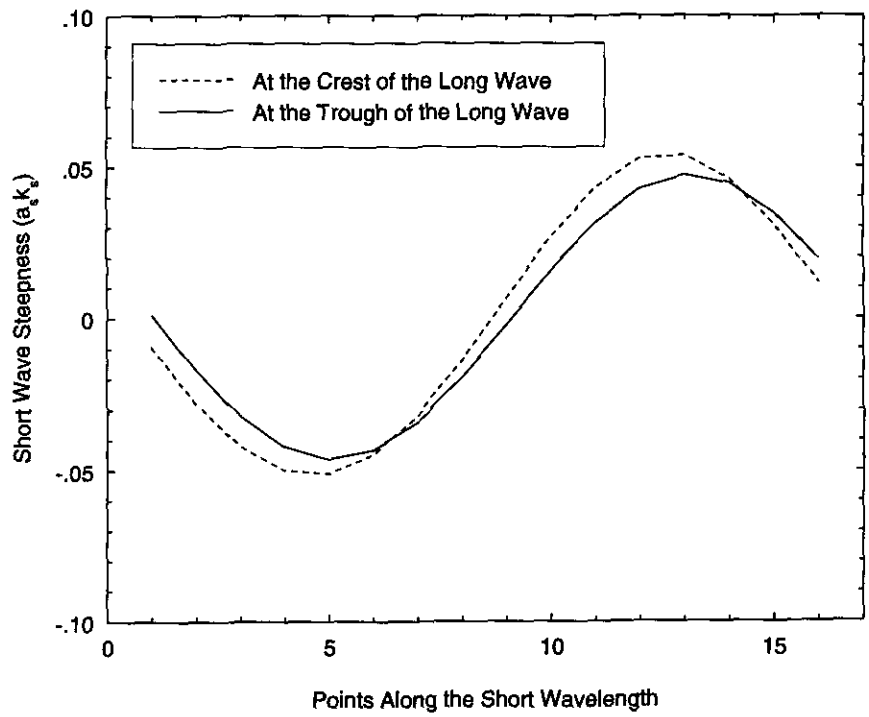

FIG. 5. Spectral method short wave profiles over the crest and trough location of a long wave of steepness 0.2 after an evolution time of one long-wave period.

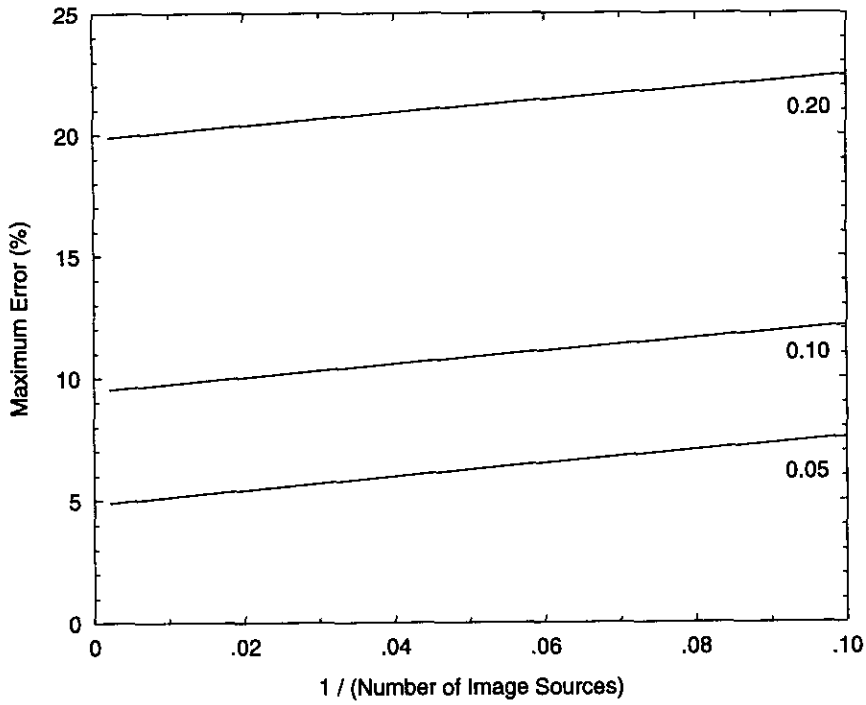

FIG. 6. Maximum edge error as a function of number of image sources.

• In long–short wave interactions, we found that the spectral method was valid for larger values of long-wave amplitude and short-wave number than might have been expected. However, as the steepness is increased, a point is reached where the spectral method becomes noticeably more erroneous than the direct method.

For wave problems with moderate steepnesses, the advantage of the spectral method is that it is computationally much more efficient than the direct method which is computationally costly, especially for three-dimensional applications. However, the availability of computers with vector hardware and large virtual memory makes the applications of the direct method, which can handle waves of larger steepnesses, practical today for some problems and will make them even more practical in the near future.

APPENDIX: EDGE ERROR FROM USE OF PERIODIC GREEN FUNCTIONS

The vertical domain faces can be eliminated by use of a doubly periodic Green function:

$$G(x, y, z; \xi, \eta, \zeta) = [(x - \xi)^2 + (y - \eta)^2 + (z - \zeta)^2]^{-1/2} + \sum_{m,n} [(x - mL - \xi)^2 + (y - nW - \eta)^2 + (z - \zeta)^2]^{-1/2}, \quad (14)$$

where $\sum_{m,n}$ denotes summation over all positive and negative integers m, n except $m = n = 0$. The dimensions of the periodic domain are represented by L and W. The approach is to consider an infinite surface around the computational domain. Inside the domain integration is done over the panels and outside the integral is approximated by the product of the singularity at the panel centroid and the panel area. The infinite sums in the above equation converge, but not so fast as to be useful for routine computation. Newman [15] has developed an efficient summation formula for the doubly-infinite sum of image sources in the interior of a rectangular channel subject to homogeneous Neumann conditions on the boundaries. His work was modified by Xu and Yue [21] to make this approach suitable for the periodic free-surface problems. However, for demonstration purposes it is more enlightening to determine the error in terms of the number of image sources. To do this, we computed the Green function with a brute force evaluation of the series for a Stokes wave problem. We varied m and n from 10 to 500 and computed the maximum error in the vertical velocity at the edge elements. Figure 6 shows the convergence with the number of image sources used in the calculations. The curves correspond to Stokes wave steepnesses of 0.05, 0.10, and 0.20 for which the maximum error converged approximately to 5, 10, and 20%, respectively. Rather large error at the edge elements is due to the fact that the influence on these points of nearby source images outside the computational domain was calculated by the product of panel area and the inverse distance, rather than the integration of the Green function over the source panel.

These errors can be reduced by using panel integration over a surface area that overlaps the computational domain, but it must be many times as large as the domain to reduce the errors to the levels achieved with our edge correction methods. This is the reason why we developed the more computationally efficient edge correction methods.

ACKNOWLEDGMENTS

This research was supported by The Office of Naval Research (ONR) (Contract N00014-89-J-1185) and by the National Science Foundation (Grant 9216788-OCE). Computations were made on a VAX 9000 at MIT; on a Cray-2 at the MIT Supercomputer Facility; and on a Cray Y-MP at the Pittsburgh Supercomputing Center which is supported by The National Science Foundation (NSF) (Grant OCE900004P).

REFERENCES

1. K. A. Brueckner and B. J. West, *J. Fluid Mech.* **196,** 585 (1988).
2. D. G. Dommermuth and D. K. P. Yue, *J. Fluid Mech.* **184,** 267 (1987).
3. D. G. Dommermuth and D. K. P. Yue, *J. Fluid Mech.* **178,** 195 (1987).
4. D. G. Dommermuth, D. K. P. Yue, W. M. Lin, R. J. Rapp, E. S. Chan, and W. K. Melville, *J. Fluid Mech.* **189,** 423 (1988).
5. J. D. Fenton, *J. Waterway, Port, Coastal Ocean Eng.* **111,** 216 (1985).
6. C. W. Gear, *Numerical Initial Value Problems in Ordinary Differential Equations* (Prentice–Hall, Englewood Cliffs, NJ, 1971).
7. S. T. Grilli and I. A. Svendsen, *Eng. Anal. Boundary Elements* **7,** 78 (1990).
8. J. L. Hess and A. M. O. Smith, Technical report, Douglas Aircraft Co., Inc., Report No. E.S. 40622, Long Beach, CA, 1962 (unpublished).
9. D. Holliday, *J. Fluid Mech.* **83,** 737 (1977).
10. W. M. Lin, J. N. Newman, and D. K. P. Yue, in *Proceedings, 15th Symposium on Naval Hydrodynamics* (The Office of Naval Research, Hamburg, Germany, 1984), p. 33.
11. M. S. Longuet-Higgins, *J. Fluid Mech.* **8,** 565 (1960).
12. M. S. Longuet-Higgins and E. D. Cokelet, *Proc. R. Soc. London Ser. A* **350,** 1 (1976).
13. P. L. Monkmeyer and J. E. Kutzbach, in *Coastal Engineering, Santa Barbara Specialty Conference, A.S.C.E, Santa Barbara, October 1965,* p. 301 (unpublished).
14. J. N. Newman, *J. Eng. Math.* **20,** 113 (1986).
15. J. N. Newman, *J. Eng. Math.* **26,** 51 (1992).
16. H. S. Ölmez, Ph.D. thesis, Massachusetts Institute of Technology, Cambridge, MA 02139, 1991 (unpublished).
17. W. H. Press, B. P. Flannery, S. A. Teukolsky, and W. T. Vetterling, *Numerical Recipes, The Art of Scientific Computing* (Cambridge Univ. Press, Cambridge, 1986).
18. J. E. Romate, Ph.D. thesis, University of Twente, Enschede, The Netherlands, 1989 (unpublished).
19. D. Sen, J. S. Pawlowski, J. Lever, and M. J. Hinchey, in *Proceedings, 18th Symposium on Naval Hydrodynamics, Ann Arbor, Michigan, August 1990,* p. 257.
20. B. J. West, K. A. Brueckner, R. S. Janda, D. M. Milder, and R. L. Milton, *J. Geophys. Res.* **92,** 11803 (1987).
21. H. Xü, Ph.D. thesis, Massachusetts Institute of Technology, Cambridge, MA 02139, 1992 (unpublished).
22. E. C. Zachmanoglou and D. W. Thoe, *Introduction to Partial Differential Equations with Applications* (Dover, New York, 1986).